


Quartz-Enhanced Photothermal-Acoustic Spectroscopy for Trace Gas Analysis

Huadan Zheng ^{1,2}, Haoyang Lin ³, Lei Dong ^{2,*} , Zhao Huang ³, Xiaohang Gu ³, Jieyuan Tang ^{1,3}, Linpeng Dong ^{1,3}, Wenguo Zhu ^{1,3}, Jianhui Yu ^{1,3,4,*} and Zhe Chen ^{1,3,4}

¹ Guangdong Provincial Key Laboratory of Optical Fiber Sensing and Communications, Department of Optoelectronic Engineering, Jinan University, Guangzhou 510632, China; zhenghuadan@126.com (H.Z.); tangjieyuan@163.com (J.T.); lpdong@jnu.edu.cn (L.D.); zhuwg88@163.com (W.Z.); thzhechen@jnu.edu.cn (Z.C.)

² State Key Laboratory of Quantum Optics and Quantum Optics Devices, Institute of Laser Spectroscopy & Collaborative Innovation Center of Extreme Optics, Shanxi University, Taiyuan 030006, China

³ Key Laboratory of Optoelectronic Information and Sensing Technologies of Guangdong Higher Education Institutes, Jinan University, Guangzhou 510632, China; linhaoyang12@gmail.com (H.L.); hhhuangzhao@foxmail.com (Z.H.); shawnkoo@foxmail.com (X.G.)

⁴ Guangdong Provincial Engineering Technology Research Center on Visible Light Communication and the Guangzhou Municipal Key Laboratory of Engineering Technology on Visible Light Communication, Jinan University, Guangzhou 510632, China

* Correspondence: donglei@sxu.edu.cn (L.D.); kensomyu@gmail.com (J.Y.); Tel.: +86-351-709-7220 (L.D.)

Received: 3 August 2019; Accepted: 18 September 2019; Published: 26 September 2019



Abstract: A crystal quartz tuning fork (QTF) was used as a detector to collect and amplify laser-induced photoacoustic and photothermal waves simultaneously for trace chemical analysis. A wavelength modulation technique was applied to the proposed quartz-enhanced photothermal-acoustic spectroscopy (QEPTAS) to improve the detection signal-to-noise ratio. The QTF detector was exposed to the illumination of a near-infrared distributed feedback laser at distances of 1 m and 2 m to evaluate the QEPTAS sensor performance. The QEPTAS sensor performance was determined by detecting water vapor in ambient air using a near-infrared distributed feedback laser with a power of ~10 mW and a wavelength of 1.39 μm . With an optimized modulation depth of 0.47 cm^{-1} , the normalized noise equivalent absorption (NNEA) coefficients of $8.4 \times 10^{-7} \text{ W} \cdot \text{cm}^{-1} \cdot \text{Hz}^{-1/2}$ and $3.7 \times 10^{-6} \text{ W} \cdot \text{cm}^{-1} \cdot \text{Hz}^{-1/2}$ were achieved for a distance of 1 m and 2 m, respectively. The developed QEPTAS technique reduces the requirements for laser beam quality, resulting in a simple but robust sensor structure and demonstrates the ability of remote sensing of gas concentrations.

Keywords: photoacoustic spectroscopy; photothermal spectroscopy; gas sensing; quartz tuning fork

1. Introduction

Photothermal spectroscopy (PTS) and photoacoustic spectroscopy (PAS) are well-established methods for experimental physics, chemistry, and biology. The history, processes, and application of PTS and PAS in gas phase analysis have previously been discussed in detail [1–3]. The photothermal and the photoacoustic effects can be divided into three stages: (1) release of heat due to the vibration–translation relaxation of molecules upon absorption of laser radiation; (2) generation of thermal and acoustic waves due to periodically heating and expansion; (3) collection and amplification of thermal and acoustic signals. According to the laws of fluid mechanics and thermodynamics, the laser-induced thermal and acoustic wave pressure p in a gas can be determined by Equation (1) [3]:

$$\partial_t^2 p(\mathbf{r}, t) - c^2 \nabla^2 p(\mathbf{r}, t) = (\sigma - 1) \partial_t H(\mathbf{r}, t), \quad (1)$$

where c , σ , and H are the sound velocity, the adiabatic coefficient of the gas, and the heat density deposited in the gas, respectively. Equation (1) has two independent solutions: Weakly damped acoustic waves with the wavelength of approximately a few centimeters and heavily damped thermal waves with the waves of approximately a few hundred micrometers [3]. The acoustic waves propagated a few centimeters and accumulated in the PAS cells. However, the thermal waves can only be detected in the vicinity of the laser beam. Usually, PAS and PTS are studied independently since the thermal and acoustic waves are separated in space.

Photoacoustic spectroscopy is an optical detection method widely used for trace gas analysis. Transducers such as microphones [4–6], cantilevers [7–10], or piezoelectric elements [11–13] were used to detect acoustic waves and convert them into mechanical or electrical signals. As a significant variant of PAS, quartz-enhanced photoacoustic spectroscopy (QEPAS) has been booming developed in the past decades [14,15]. In QEPAS, a quartz tuning fork (QTF) with a specific resonance frequency of ~ 32 kHz and an extremely high Q factor value of $\sim 10,000$ was used to collect the acoustic waves and accumulate the acoustic energy [16–18]. Because of the high resonance frequency of >10 kHz, the narrow resonance spectra of ~ 4 Hz, and the quadrupole electrode pattern of the QTF, QEPAS is immune to the background acoustic noise which results in a high detection signal-to-noise ratio and sensitivity [15]. The gas sensor based on the QEPAS technique has been applied for chemical analysis [19–22], atmospheric monitoring [23–27], and biological diagnostics [28–30].

As with photoacoustic spectroscopy, photothermal spectroscopy is an indirect method for measuring the change in the thermal states of the sample that is induced by the absorption of laser radiation. Examples of photothermal techniques include photothermal interferometry (PTI), photothermal lensing (PTL), and photothermal deflection (PTD). With the merits of zero-reference and laser power dependence, photothermal spectroscopy is highly sensitive. Traditional thermally sensitive transducers include pyroelectric crystals, bolometers, and microelectromechanical systems (MEMS). Most recently, a highly sensitive PTS technology called quartz-tuning-fork enhanced photothermal spectroscopy (QEPTS) was developed for trace gas analysis by use of a QTF [31]. A QTF was used as the high-performance transducer to convert the photothermal signals to electrical signals. The laser beam passed through a 20 cm-long gas-sampling cell and then was focused on the QTF prong. The heat released by the target molecules upon absorption of the laser radiation was collected by the QTF. The heat expansion drove the QTF to vibrate. Then the resonance of the QTF amplified the signal. In QEPAS, the laser beam must be collimated to pass through the spacing of ~ 300 μm without touching the QTF prongs. In QEPTS, the laser beam was focused on a spot with the diameter of ~ 36 μm , located in a particular area of the QTF prong where no silver layer was coated.

In this manuscript, quartz-enhanced photothermal-acoustic spectroscopy (QEPTAS) was developed for trace gas analysis. In QEPTAS, the laser beam illuminates the QTF prong spacing and the prong surface simultaneously. The excitation of a QTF consisted of two elements: Photoacoustic waves and photothermal waves. A commercially available 32 kHz QTF was used as a detector to collect and amplify the laser-induced acoustic waves and thermal waves simultaneously. There is no focus lens for laser beam shaping in QEPTAS, thus simplifying the gas sensor structure. QEPTAS removes the requirement for laser beam quality and provides the possibility of the remote sensing of gas concentrations.

2. Experiments and Results

The schematic diagram of the QEPTAS experimental setup is depicted in Figure 1. A 1.37 μm near-infrared fiber-coupled distributed feedback (DFB) diode laser was employed as the excitation source to detect water vapor (H_2O) in ambient air. The temperature and current of the diode laser can be controlled by a high-stability laser diode controller (ILX Lightwave). A two-channel arbitrary waveform function generator (Tektronix AFG3102) was used to produce a ramp signal with the frequency of 10 mHz and a sine signal with the frequency of $f_0/2$, where f_0 corresponds to the resonance frequency of the QTF. The $2f$ wavelength modulation technique has the advantage of tunability and modulation capabilities of DFB lasers, improving the sensor performance [32].

The QTF was fixed on an XYZ linear stage and positioned in a cap, not shown in Figure 1. The acoustic and thermal waves induced by the laser radiation drove the QTF to vibrate. The electric signals generated by the piezoelectric effect in quartz was processed by a custom transimpedance preamplifier with a feedback resistance of 10 M Ω and then were fed to a lock-in amplifier (Stanford SR830) to demodulate the signal in $2f$ mode. A Labview™ program was used to control the experimental system and retrieve the gas concentrations from the obtained $2f$ signal [24]. The experiment was conducted at a local atmospheric pressure of ~ 933 hPa (700 Torr) and room temperature of ~ 25 °C.

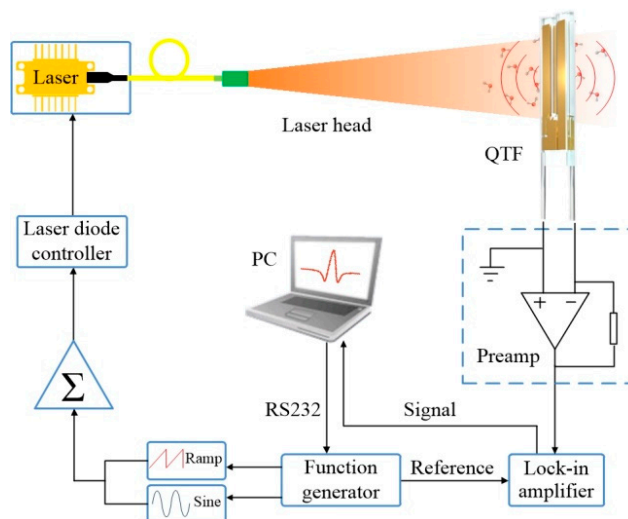


Figure 1. Experimental setup of quartz-enhanced photothermal-acoustic spectroscopy. Σ : Adder, PC: Personal computer, Preamp: Pre-amplifier; QTF: Quartz tuning fork. RS232: A standard protocol used for serial communication.

As proof of concept, a pigtailed laser diode with the beam M^2 factor of 1.258 was used as the excitation source. Compared to previous publications on QEPAS and QEPTS, a non-focusing light source was firstly used in the experiment. The beam quality of the laser was analyzed by a dual scanning slit beam profiler (Thorlabs BP209-IR/M) with a beam diameter error $<10\%$. The beam diameter as a function of laser head position is plotted in Figure 2. The distance between the laser head and the slit of the beam profiler changed from 5 mm to up to ~ 1 m. The laser temperature and injection current were set to 23 °C and 40 mA, respectively, corresponding to the emission power of 6.7 mW. When the position of the beam profiler was 955 mm, the beam diameter reached ~ 10 mm, corresponding to a beam spot about 100 times that used in the conventional QEPAS. The edge of the beam profile was defined as the position where the intensity fell to $1/e^2$ of the maximum value at the center.

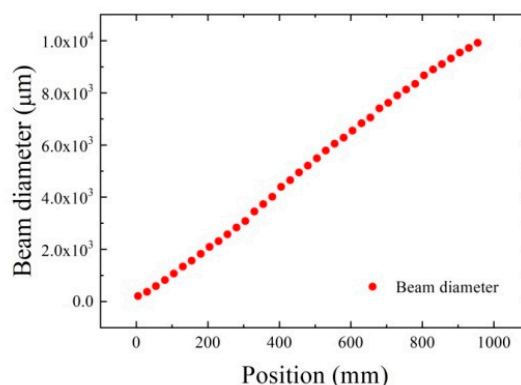


Figure 2. Laser beam quality analysis at a distance of up to 1 m. The beam diameter error of 10% was determined by the beam profiler.

In order to investigate the photothermal-acoustic response of the QTF surface to the laser beam, the normalized QEPTAS signal amplitude, as a function of x_0 , was researched. Figure 3a shows the diagram of QEPTAS. The QTF was fixed at the position of 150 μm from the laser head; y_0 of the laser spot was set to 0.7 mm from the QTF opening; x_0 of the laser spot was changed from 0 to 800 μm by use of an XYZ translation stage with the precision of 10 μm , as shown in Figure 3b. The prong length of the QTF, defined as the distance from the QTF opening to the x-axis, was measured to be ~ 3.6 mm. The prong spacing of the QTF was measured to be ~ 0.3 mm. The QTF prong width, defined as the distance from Line A to Line C, was measured to be ~ 0.6 mm. QEPTAS obtained the maximum signal amplitude when the laser spot was positioned at the center of the QTF prong spacing. When the position of the laser spot moved horizontally to the edge of the QTF prong (Line A), the signal amplitude decreased by $\sim 23\%$. The minimum signal amplitude was obtained when the laser spot was positioned at the center of the QTF prong (Line B). For higher values, the signal amplitude increased to $\sim 40\%$ of the maximum value at Line C. The signal variation is related to the electrode layer pattern on the QTF surface. Most of the area of the QTF prong is coated with a silver layer, which has a high reflectivity for the laser beam [31]. There was no coating in the vicinity of Line A and Line C, which means that more photons were absorbed by the QTF, resulting in a higher signal amplitude. The subsequent decrease beyond Line C was due to the decrease of photothermal effects on the QTF surface.

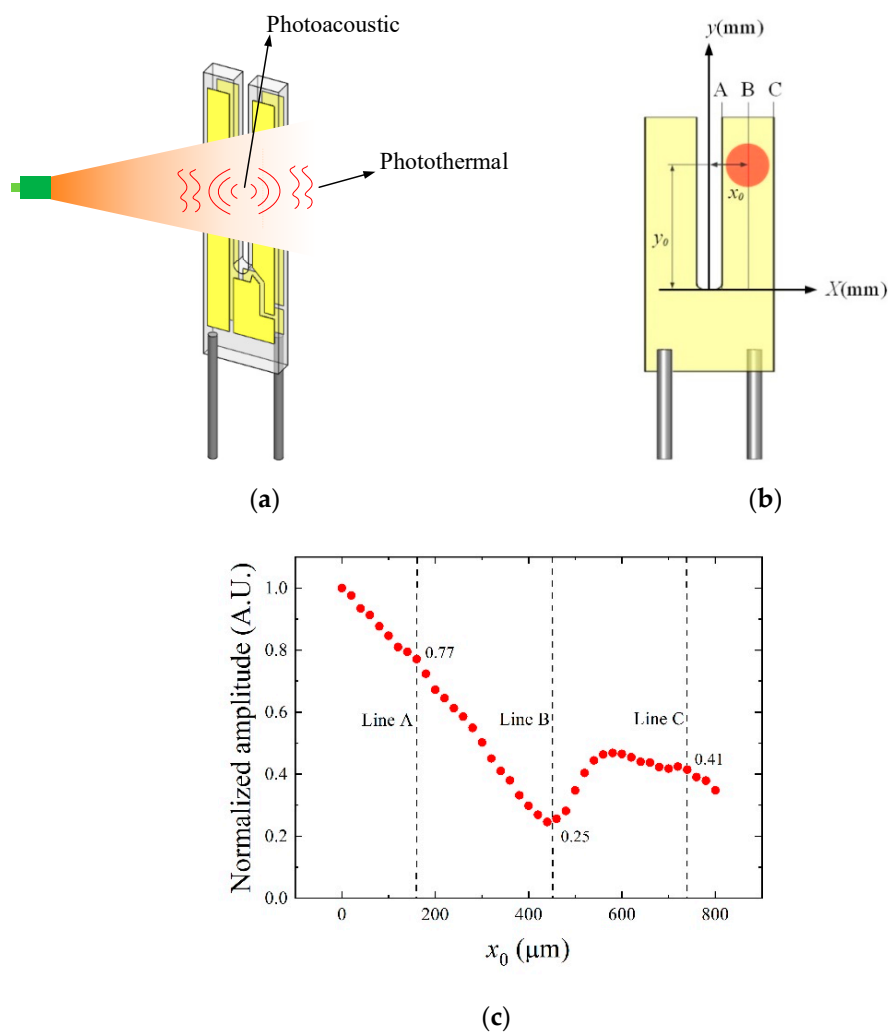


Figure 3. (a) Diagram of quartz-enhanced photothermal-acoustic spectroscopy. (b) Lines A, B, C represent the edges and central line of the QTF prong, respectively. The values of x_0 and y_0 represent the distance between the laser-spot center and the QTF y -axis and x -axis, respectively. (c) The normalized

quartz-enhanced photothermal-acoustic spectroscopy (QEPTAS) signal amplitude as a function of laser spot position, x_0 . The error of amplitude was less than 1%.

In order to determine the optimum laser excitation of the QEPTAS system, the laser wavelength modulation depth was varied from 0.2 cm^{-1} to 0.65 cm^{-1} to obtain a maximum $2f$ QEPTAS signal amplitude. The experimental results shown in Figure 4 illustrate the influence of the laser modulation depth on the QEPTAS signal. In the wavelength modulation, the theoretical modulation index m , defined as the ratio between the modulation depth and the half width at half maximum of the absorption profile, was ~ 2.2 , violating the hypothesis of the Taylor series expansions [33]. However, the optimal modulation depth to achieve the maximum signal needs to be optimized experimentally. The signal amplitude increased monotonically with the laser modulation depth and, for values higher than 0.47 cm^{-1} , the signal amplitude increased only by $<1\%$. The $2f$ signal amplitude started to decrease when the modulation depth was larger than 0.55 cm^{-1} . Therefore, the optimum laser modulation depth was $\sim 0.47 \text{ cm}^{-1}$.

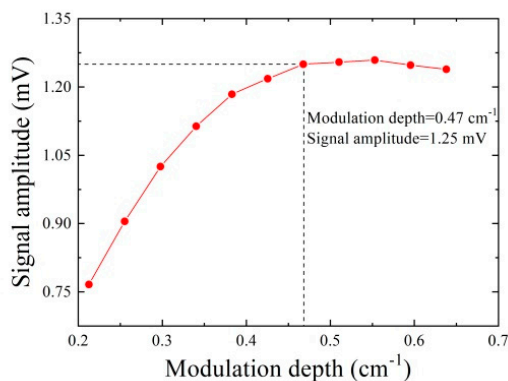


Figure 4. Optimization of laser modulation depth.

The performance of the QEPTAS sensor was evaluated by detecting H_2O in ambient air. The QEPTAS acoustic detection module (ADM) was positioned at distances of 1 m and 2 m from the laser head. The emission wavelength of the laser was tuned from 7306.31 cm^{-1} to 7308.01 cm^{-1} to target the H_2O absorption line at 7306.75 cm^{-1} , with a line intensity of $1.8 \times 10^{-20} \text{ cm/molecule}$. Figure 5 shows the QEPTAS signal amplitude of $1.25 \times 10^{-3} \text{ V}$ and $2.4 \times 10^{-4} \text{ V}$, corresponding to the QEPTAS ADM distances of 1 m and 2 m, respectively. The 1σ noise was obtained by changing the laser injection current to tune the emission wavelength away from the H_2O absorption line. The calculated 1σ standard deviation for distances of 1 m and 2 m were $1.19 \mu\text{V}$ and $1.02 \mu\text{V}$, respectively. The ambient H_2O concentration of 1.3% was determined by direct absorption spectroscopy [34]. For Figure 5, the measurement took $\sim 5 \text{ min}$.

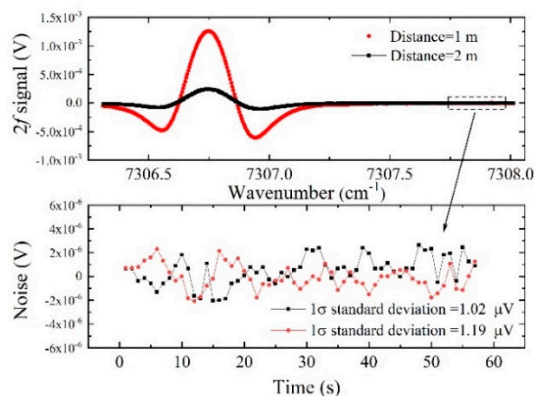


Figure 5. Optimized QEPTAS $2f$ signal obtained at distances of 1 m and 2 m.

The calculation of the normalized noise equivalent absorption (NNEA) coefficient is given by Equation (2):

$$NNEA = \frac{a_{\min} P_0}{\sqrt{\Delta f}}, \quad (2)$$

where a_{\min} , P_0 , and Δf are the minimum detectable absorption coefficient at an SNR = 1, the laser optical power, and the equivalent noise detection bandwidth, respectively [35]. The detection limits for H₂O obtained by the QEPTAS sensor at distances of 1 m and 2 m were ~12 ppm and ~55 ppm, corresponding to a NNEA coefficients of $8.4 \times 10^{-7} \text{ W} \cdot \text{cm}^{-1} \cdot \text{Hz}^{-1/2}$ and $3.7 \times 10^{-6} \text{ W} \cdot \text{cm}^{-1} \cdot \text{Hz}^{-1/2}$, respectively. Compared to other photothermal spectroscopy techniques based on a silicon resonator [36] or a fiber-coupled Fabry–Pérot interferometer [37], the NNEA of QEPTAS is competitive. Yufei Ma et al. give a brief qualitative description of the analysis of photothermal effects [31]. The detailed theoretical analysis can be obtained from a theoretical model for resonant optoacoustic systems [38].

3. Conclusions

The proposed QEPTAS is a useful tool for the investigation of photoacoustic and photothermal effects simultaneously. The commercially available QTF acted as a highly sensitive detector to collect the acoustic and thermal waves upon the absorption of laser radiation by target molecules. The remote sensing ability of the QEPTAS sensor was demonstrated by detecting H₂O in ambient air. The feature of non-contact detection and the lack of laser beam shaping components of the QEPTAS sensor introduced a better error tolerance than that of QEPAS and QEPTS in sensor assembling. The QEPTAS sensor shows great potential for application in the recently developed room-temperature continuous terahertz quantum cascade lasers [39,40], which are not easily used in QEPAS or QEPTS, since in QEPAS and QEPTS, the focused laser spot diameter d is limited by the diffraction limit $d = \lambda/2 \times \text{NA}$, where NA represents the numerical aperture. The wavelength λ can be up to centimeters. The advantage of QTF is that the overall size of a typical sensor platform can be significantly reduced to a size that is suitable for applications requiring lightweight and compact structures, such as balloons or unmanned aerial vehicles (UAV) [41]. Further improvement can be made by utilizing custom tuning forks made of materials with higher piezoelectric and thermoelectric coefficients than a commercial quartz tuning fork.

Author Contributions: H.Z. and L.D. (Lei Dong), methodology; L.D. (Linpeng Dong), software, H.L., validation; Z.H., formal analysis; H.Z., investigation and data curation; X.G., Writing—Original draft preparation; H.Z., Writing—Review and editing; L.D. (Lei Dong), supervision; J.Y., project administration; J.T., L.D. (Linpeng Dong) and W.Z., funding acquisition; H.Z., J.Y. and Z.C.

Funding: This work is supported by the National Natural Science Foundation of China (11004086, 61675092, 61275046, 61475066, 61405075, 61601404), Natural Science Foundation of Guangdong Province (2016A030313079, 2016A030310098, 2016A030311019, 2014A030313377, 2015A030306046, 2015A030313320), Special Funds for Major Science and Technology Projects of Guangdong Province (2019B010138004, 2014B010120002, 2014B010117002, 2015B010125007), Project of Guangzhou Industry Leading Talents (CXLJTD-201607), and Planned Science & Technology Project of Guangzhou (2017A010102006, 2016A010101017, 2016B010111003, 201506010046), Joint fund of pre-research for equipment, Ministry of Education of China (6141A02022124), Aeronautical Science Foundation of China (201708W4001); Foundation for Distinguished Young Talents in Higher Education of Guangdong (2018KQNCX009, 2018KQNCX279), the Fundamental Research Funds for the Central Universities (21619402), State Key Laboratory of Applied Optics (SKLAO-201914).

Conflicts of Interest: The authors declare no conflict of interest.

References

1. Bailey, R.T.; Bernegger, S.; Bicanic, D.; Bijnen, F.; Blom, C.W.P.M.; Cruickshank, F.R.; Diebold, G.J.; Fiedler, M.; Harren, F.; Hess, P.; et al. *Photoacoustic, Photothermal and Photochemical Processes in Gases*; Springer: Berlin/Heidelberg, Germany, 1989; pp. 1–252.
2. Coufal, H.; McClelland, J.F. Photothermal and photoacoustic spectroscopy. *J. Mol. Struct.* **1988**, *173*, 129–140. [[CrossRef](#)]

3. Miklós, A.; Hess, P.; Bozóki, Z. Application of acoustic resonators in photoacoustic trace gas analysis and metrology. *Rev. Sci. Instrum.* **2001**, *72*, 1937–1955. [[CrossRef](#)]
4. Kottmann, J.; Rey, J.M.; Sigrist, M.W. Mid-Infrared photoacoustic detection of glucose in human skin: Towards non-invasive diagnostics. *Sensors* **2016**, *16*, 1663. [[CrossRef](#)] [[PubMed](#)]
5. Zoltán, B.; Pogány, A.; Szabó, G. Photoacoustic instruments for practical applications: Present, potentials, and future challenges. *Appl. Spectrosc. Rev.* **2001**, *46*, 1–37.
6. Bauer, R.; Stewart, G.; Johnstone, W.; Boyd, E.; Lengden, M. 3D-printed miniature gas cell for photoacoustic spectroscopy of trace gases. *Opt. Lett.* **2014**, *39*, 4796–4799. [[CrossRef](#)] [[PubMed](#)]
7. Hirschmann, C.B.; Lehtinen, J.; Uotila, J.; Ojala, S.; Keiski, R.L. Sub-ppb detection of formaldehyde with cantilever enhanced photoacoustic spectroscopy using quantum cascade laser source. *Appl. Phys. B* **2013**, *111*, 603–610. [[CrossRef](#)]
8. Adamson, B.D.; Sader, J.E.; Bieske, E.J. Photoacoustic detection of gases using microcantilevers. *J. Appl. Phys.* **2009**, *106*, 114510. [[CrossRef](#)]
9. Khan, D.; Bayram, F.; Gajula, D.; Talukdar, A.; Li, H.; Koley, G. Plasmonic amplification of photoacoustic waves detected using piezotransistive GaN microcantilevers. *Appl. Phys. Lett.* **2017**, *111*, 062102. [[CrossRef](#)]
10. Gong, Z.; Chen, K.; Yang, Y.; Zhou, X.; Peng, W.; Yu, Q. High-sensitivity fiber-optic acoustic sensor for photoacoustic spectroscopy based traces gas detection. *Sens. Actuators B Chem.* **2017**, *247*, 290–295. [[CrossRef](#)]
11. Van Neste, C.W.; Senesac, L.R.; Thundat, T. Standoff photoacoustic spectroscopy. *Appl. Phys. Lett.* **2008**, *92*, 234102. [[CrossRef](#)]
12. Ngai, A.K.Y.; Persijn, S.T.; Lindsay, I.D.; Kosterev, A.A.; Groß, P.; Lee, C.J.; Cristescu, S.M.; Tittel, F.K.; Boller, K.-J.; Harren, F.J.M. Continuous wave optical parametric oscillator for quartz-enhanced photoacoustic trace gas sensing. *Appl. Phys. B* **2007**, *89*, 123. [[CrossRef](#)]
13. Liu, K.; Cao, Y.; Wang, G.; Zhang, W.; Chen, W.; Gao, X. A novel photoacoustic spectroscopy gas sensor using a low cost polyvinylidene fluoride film. *Sens. Actuators B Chem.* **2018**, *277*, 571–575. [[CrossRef](#)]
14. Kosterev, A.A.; Bakhirkin, Y.A.; Curl, R.F.; Tittel, F.K. Quartz-enhanced photoacoustic spectroscopy. *Opt. Lett.* **2002**, *27*, 1902–1904. [[CrossRef](#)] [[PubMed](#)]
15. Patimisco, P.; Sampaolo, A.; Dong, L.; Tittel, F.K.; Spagnolo, V. Recent advances in quartz enhanced photoacoustic sensing. *Appl. Phys. Rev.* **2018**, *5*, 011106. [[CrossRef](#)]
16. Wu, H.; Dong, L.; Zheng, H.; Yu, Y.; Ma, W.; Zhang, L.; Yin, W.; Xiao, L.; Jia, S.; Tittel, F.K. Beat frequency quartz-enhanced photoacoustic spectroscopy for fast and calibration-free continuous trace-gas monitoring. *Nat. Commun.* **2017**, *8*, 15331. [[CrossRef](#)] [[PubMed](#)]
17. Ma, Y.; Lewicki, R.; Razeghi, M.; Tittel, F.K. QEPAS based ppb-level detection of CO and N₂O using a high power CW DFB-QCL. *Opt. Express* **2013**, *21*, 1008–1019. [[CrossRef](#)] [[PubMed](#)]
18. Dong, L.; Kosterev, A.A.; Thomazy, D.; Tittel, F.K. QEPAS spectrophones: Design, optimization, and performance. *Appl. Phys. B* **2010**, *100*, 627–635. [[CrossRef](#)]
19. Wysocki, G.; Kosterev, A.A.; Tittel, F.K. Influence of molecular relaxation dynamics on quartz-enhanced photoacoustic detection of CO₂ at $\lambda = 2 \mu\text{m}$. *Appl. Phys. B* **2006**, *85*, 301–306. [[CrossRef](#)]
20. Wang, Z.; Geng, J.; Ren, W. Quartz-Enhanced Photoacoustic Spectroscopy (QEPAS) Detection of the ν_7 Band of Ethylene at Low Pressure with CO₂ Interference Analysis. *Appl. Spectrosc.* **2017**, *71*, 1834–1841. [[CrossRef](#)]
21. Giglio, M.; Patimisco, P.; Sampaolo, A.; Zifarelli, A.; Blanchard, R.; Pfluegl, C.; Witinski, M.F.; Vakhshoori, D.; Tittel, F.K.; Spagnolo, V. Nitrous oxide quartz-enhanced photoacoustic detection employing a broadband distributed-feedback quantum cascade laser array. *Appl. Phys. Lett.* **2018**, *113*, 171101. [[CrossRef](#)]
22. Spagnolo, V.; Dong, L.; Kosterev, A.A.; Tittel, F.K. Modulation cancellation method for isotope ¹⁸O/¹⁶O ratio measurements in water. *Opt. Express* **2012**, *20*, 3401–3407. [[CrossRef](#)] [[PubMed](#)]
23. Yi, H.; Maamary, R.; Gao, X.; Sigrist, M.W.; Fertein, E.; Chen, W. Short-lived species detection of nitrous acid by external-cavity quantum cascade laser based quartz-enhanced photoacoustic absorption spectroscopy. *Appl. Phys. Lett.* **2015**, *106*, 101109. [[CrossRef](#)]
24. Zheng, H.; Dong, L.; Yin, X.; Liu, X.; Wu, H.; Zhang, L.; Ma, W.; Yin, W.; Jia, S. Ppb-level QEPAS NO₂ sensor by use of electrical modulation cancellation method with a high power blue LED. *Sens. Actuators B Chem.* **2015**, *208*, 173–179. [[CrossRef](#)]

25. Wu, H.; Dong, L.; Yin, X.; Sampaolo, A.; Patimisco, P.; Ma, W.; Zhang, L.; Yin, W.; Xiao, L.; Spagnolo, V.; et al. Atmospheric CH₄ measurement near a landfill using an ICL-based QEPAS sensor with VT relaxation self-calibration. *Sens. Actuators B Chem.* **2019**, *297*, 126753. [[CrossRef](#)]
26. Rück, T.; Bierl, R.; Matysik, F.M. NO₂ trace gas monitoring in air using off-beam quartz enhanced photoacoustic spectroscopy (QEPAS) and interference studies towards CO₂, H₂O and acoustic noise. *Sens. Actuators B Chem.* **2018**, *255*, 2462–2471. [[CrossRef](#)]
27. Jahjah, M.; Jiang, W.; Sanchez, N.P.; Ren, W.; Patimisco, P.; Spagnolo, V.; Herndon, S.C.; Griffin, R.J.; Tittel, F.K. Atmospheric CH₄ and N₂O measurements near Greater Houston area landfills using a QCL-based QEPAS sensor system during DISCOVER-AQ 2013. *Opt. Lett.* **2014**, *39*, 957–960. [[CrossRef](#)] [[PubMed](#)]
28. Köhring, M.; Böttger, S.; Willer, U.; Schade, W. LED-absorption-QEPAS sensor for biogas plants. *Sensors* **2015**, *15*, 12092–12102. [[CrossRef](#)] [[PubMed](#)]
29. Nguyen Ba, T.; Triki, M.; Desbrosses, G.; Vicet, A. Quartz-enhanced photoacoustic spectroscopy sensor for ethylene detection with a 3.32 μ m distributed feedback laser diode. *Rev. Sci. Instrum.* **2015**, *86*, 023111. [[CrossRef](#)]
30. Wang, Z.; Li, Z.; Ren, W. Quartz-enhanced photoacoustic detection of ethylene using a 10.5 μ m quantum cascade laser. *Opt. Express* **2016**, *24*, 4143–4154. [[CrossRef](#)]
31. Ma, Y.; He, Y.; Tong, Y.; Yu, X.; Tittel, F.K. Quartz-tuning-fork enhanced photothermal spectroscopy for ultra-high sensitive trace gas detection. *Opt. Express* **2018**, *26*, 32103–32110. [[CrossRef](#)]
32. Schilt, S.; Thevenaz, L.; Robert, P. Wavelength modulation spectroscopy: Combined frequency and intensity laser modulation. *Appl. Opt.* **2003**, *42*, 6728–6738. [[CrossRef](#)] [[PubMed](#)]
33. Patimisco, P.; Sampaolo, A.; Bidaux, Y.; Bismuto, A.; Scott, M.; Jiang, J.; Muller, A.; Faist, J.; Tittel, F.K.; Spagnolo, V. Purely wavelength-and amplitude-modulated quartz-enhanced photoacoustic spectroscopy. *Opt. Express* **2016**, *24*, 25943–25954. [[CrossRef](#)] [[PubMed](#)]
34. Yin, X.; Dong, L.; Zheng, H.; Liu, X.; Wu, H.; Yang, Y.; Ma, W.; Zhang, L.; Yin, W.; Xiao, L.; et al. Impact of humidity on quartz-enhanced photoacoustic spectroscopy based CO detection using a near-IR telecommunication diode laser. *Sensors* **2016**, *16*, 162. [[CrossRef](#)] [[PubMed](#)]
35. Elia, A.; Di Franco, C.; Spagnolo, V.; Lugarà, P.M.; Scamarcio, G. Quantum cascade laser-based photoacoustic sensor for trace detection of formaldehyde gas. *Sensors* **2009**, *9*, 2697–2705. [[CrossRef](#)] [[PubMed](#)]
36. Vasiliev, A.; Malik, A.; Muneeb, M.; Kuyken, B.; Baets, R.; Roelkens, G. On-chip mid-infrared photothermal spectroscopy using suspended silicon-on-insulator microring resonators. *ACS Sens.* **2016**, *1*, 1301–1307. [[CrossRef](#)]
37. Breitegger, P.; Lang, B.; Bergmann, A. Intensity modulated photothermal measurements of NO₂ with a compact fiber-coupled Fabry–Pérot interferometer. *Sensors* **2019**, *19*, 3341. [[CrossRef](#)]
38. Petra, N.; Zweck, J.; Minkoff, S.E.; Kosterev, A.A.; Doty, J.H., III. Modeling and design optimization of a resonant optoacoustic trace gas sensor. *SIAM J. Appl. Math.* **2011**, *71*, 309–332. [[CrossRef](#)]
39. Patimisco, P.; Sampaolo, A.; Zheng, H.; Dong, L.; Tittel, F.K.; Spagnolo, V. Quartz-enhanced photoacoustic spectrophones exploiting custom tuning forks: A review. *Adv. Phys. X* **2017**, *2*, 169–187. [[CrossRef](#)]
40. Jung, S.; Jiang, A.; Jiang, Y.; Vijayraghavan, K.; Wang, X.; Troccoli, M.; Belkin, M.A. Broadly tunable monolithic room-temperature terahertz quantum cascade laser sources. *Nat. Commun.* **2014**, *5*, 4267. [[CrossRef](#)]
41. Ma, Y. Review of recent advances in QEPAS-based trace gas sensing. *Appl. Sci.* **2018**, *8*, 1822. [[CrossRef](#)]

